Thermoelectric performance of Li doped, p-type $Mg_2(Ge,Sn)$ and comparison with $Mg_2(Si,Sn)$

J. de Boor[1+], U. Saparamadu[2+], J. Mao[2], K. Dahal[2], E. Müller[1,3], Zhifeng Ren[2*]

1: Institute of Materials Research, German Aerospace Center, 51147 Koeln, Germany

2: Department of Physics and Texas Center for Superconductivity, University of Houston, Houston, TX 77204, USA

3: Institute of Inorganic and Analytical Chemistry, Justus Liebig University Giessen, 35392 Giessen, Germany

+: contributed equally

Johannes.deboor@dlr.de, zren@uh.edu

Abstract:

Solid solutions with chemical formula $Mg_2(Si,Ge,Sn)$ are promising thermoelectric materials with very good properties for the n-type material but significantly worse for the p-type. For power generation applications good n- and p-type materials are required and it has been shown recently that Li doping can enhance the carrier concentration and improve the thermoelectric properties for p-type $Mg_2Si_{1-x}Sn_x$. We have investigated the potential of p-type $Mg_2(Ge,Sn)$ by optimizing $Mg_2Ge_{0.4}Sn_{0.6}$ using Li as dopant. We were able to achieve high carrier concentrations (1.4×10^{20} cm^{-3}) and relatively high hole mobilities resulting in high power factors of 1.7×10^{-3} $W\ m^{-1}\ K^{-2}$ at 700 K, the highest value reported so far for this class of material. Exchanging Ge by Si allows for a systematic comparison of $Mg_2(Ge,Sn)$ with $Mg_2(Si,Sn)$ and shows that Si containing samples exhibit a lower power factor but also a lower thermal conductivity resulting in comparable thermoelectric figure-of-merit. The data is furthermore analyzed in the framework of a single parabolic band model to gain insight on the effect of composition on band structure.

1. Introduction

Thermoelectric materials can be used to convert (waste) heat directly into electrical energy. They can thus power autonomous devices or enhance the energy efficiency of various applications and industrial processes [1]. The efficiency of the heat to electrical energy conversion is linked to the thermoelectric figure of merit of the materials, given by $ZT = \frac{\sigma S^2}{\kappa} T$, here σ is the electrical conductivity, κ the thermal conductivity, S the Seebeck coefficient, and T the absolute temperature. A large fraction of the potentially available waste heat can be found in the mid-temperature region

between 500 K and 800 K for which several material classes with attractive thermoelectric properties with $ZT > 1$ can be considered, *e.g.,* nanostructured PbTe [2], $CoSb_3$ based skutterudites [3], half Heusler [4], SnSe [5], Cu_2Se based materials [6], and Mg_2Si based solid solutions [7-13]. Among these, Mg_2Si-based solid solutions have the crucial advantage of abundant and non-toxic constituting elements. This makes them one of the most attractive material classes also from an economical point of view [14]. A further material class specific advantage is their low density which is a factor of 2-3 lower than that of skutterudites or PbTe. This holds especially for the binary or Si-rich compositions [15-17] and gives magnesium silicides an advantage where weight is crucial, *i.e.*, in airborne or mobile applications.

Furthermore, magnesium silicides are a technologically relatively advanced material class with systematic contacting studies available [18-22], fabrication and analysis of lab prototypes for thermoelectric modules [23-28] and companies like Alphabet Energy commercializing Mg_2Si-based thermoelectric generators.

However, the excellent thermoelectric properties have been reported only for n-type material, with the p-type being clearly inferior [29, 30]. Various dopants have been used to synthesize p-type material [31, 32]. Some like Ag are found to be unstable at higher T leading to mixed conduction [33], while others induce holes into the material but far less than expected thus leading to unoptimized material due to too low carrier concentrations. Based on earlier work of Isoda *et al*. [34], it has been shown recently by Zhang *et al*. that Li can be employed as an effective dopant in $Mg_2Si_{0.3}Sn_{0.7}$ resulting in carrier concentrations up to $n \approx 5 \times 10^{20}$ cm^{-3} and a significantly enhanced figure of merit with $ZT_{max} \approx 0.5$ [35]. Tang *et al*. and Gao *et al*. furthermore showed that Li can also be employed with $Mg_2Si_{0.4}Sn_{0.6}$ leading to slightly enhanced thermoelectric properties with $ZT_{max} \approx 0.6$ [36, 37]. For the n-type material it has been shown that $Mg_2(Ge,Sn)$ has thermoelectric properties comparable to $Mg_2(Si,Sn)$ with the additional advantage that the power factors are systematically larger [38, 39]. It is thus the superior material for applications where output power is the main concern, in addition to efficiency. For the p-type material no reports of $Mg_2(Ge,Sn)$ using Li as dopant are available. We have therefore synthesized Li-doped $Mg_2Ge_{0.4}Sn_{0.6}$ using mechanical alloying of the elements. This synthesis technique is well established for the n-type material as it largely avoids Mg-loss and oxidation issues that are often a problem with liquid synthesis techniques [38-40]. We can show that Li is a relatively effective dopant for $Mg_2Ge_{0.4}Sn_{0.6}$ allowing for $n > 10^{20} cm^{-3}$ and $ZT_{max} > 0.5$. We have furthermore synthesized Li-doped $Mg_2Si_{0.4}Sn_{0.6}$ samples using the same synthesis route allowing for a systematic study of the effect of two elements. Further comparison with literature data leads to some understanding of the influence of the (Si/Ge):Sn ratio on thermoelectric properties, band structure and dopant solubility.

2. Experimental

The desired elements (Magnesium turning (Mg, 99.98%; Alfa Aesar), tin shots and powder (Sn, 99.8%; Alfa Aesar), germanium pieces (Ge, 99.9999%; Alfa Aesar), silicon granule (Si, 99.999%; Alfa Aesar), and Li shots (99.9%, Alfa Aesar) were loaded into a stainless steel jar in a glove box according to the desired composition and a total mass of 10 g. No excess Mg was added. The elements were ball milled in a Spex 8000 high energy ball mill for a total time of 20 h. During the 20 h the jar was

usually inspected 3 times to clear macroscopic inhomogeneity that might have formed during ball milling. After 20 h the powder was of bluish appearance and no inhomogeneity was apparent. Cylindrical pellets were compacted using current assisted sintering with a sintering temperature of 1023 K, a holding time of 2 min, a heating rate of 100 K/min and a pressure of 60 MPa. Temperature dependent electrical conductivity and Seebeck coefficient data was obtained using a ZEM-3, while the thermal conductivity was obtained as the product of the thermal diffusivity D measured by a laser flash measurement system (Netzsch, LFA 457), the mass density ρ by Archimedes' principle, and the specific heat c_p by differential scanning calorimetry (Netzsch, DSC 404 C). The experimental results for the specific heat was averaged for all $Mg_2Ge_{0.4}Sn_{0.6}$ samples and the mean values were used to calculate the thermal conductivity $\kappa = D\rho c_p$; the same was done for the $Mg_2Si_{0.4}Sn_{0.6}$ samples. The precision of S and σ is estimated to be 5%, while the absolute error may be larger [41]. For the κ measurement the uncertainty is estimated to 10%. Hall coefficients were measured at room temperature using a PPMS (Quantum Design, PPMS Dynacool) and a single carrier type was assumed for calculation of carrier density and carrier mobility. X-ray diffraction (XRD) data was obtained using a Siemens D5000 and Rietveld refinement of the lattice parameters a was performed using Topas 4.2. SEM images were taken using a Zeiss Ultra 55 equipped with an energy dispersive X-ray (EDX) detector.

3. Results

A list of samples with nominal compositions and room temperature transport properties is given in Table I.

Table I: List of $Mg_2Ge_{0.4}Sn_{0.6}$ and $Mg_2Si_{0.4}Sn_{0.6}$ samples with nominal compositions, Li content x, as well as some room temperature properties.

Composition	Li content x	$n_H/$ 10^{19} cm^{-3}	μ_H / $cm^2V^{-1}s^{-1}$	Density $\rho/$ $g\,cm^{-3}$	Red. chem. pot η	$L/10^{-8}$ $W\,\Omega\,K^{-2}$
$Mg_{1.995}Li_{0.005}Ge_{0.4}Sn_{0.6}$	0.005	5.9	53	3.32	1.2	1.75
$Mg_{1.99}Li_{0.01}Ge_{0.4}Sn_{0.6}$	0.01	6.8	48	3.38	1.5	1.79
$Mg_{1.98}Li_{0.02}Ge_{0.4}Sn_{0.6}$	0.02	11.1	39	3.35	2.1	1.87
$Mg_{1.97}Li_{0.03}Ge_{0.4}Sn_{0.6}$	0.03	12.6	42	3.36	2.2	1.89
$Mg_{1.96}Li_{0.04}Ge_{0.4}Sn_{0.6}$	0.04	12.9	38	3.36	2.2	1.88
$Mg_{1.94}Li_{0.06}Ge_{0.4}Sn_{0.6}$	0.06	12.3	38	3.32	2.4	1.91
$Mg_{1.99}Li_{0.01}Si_{0.4}Sn_{0.6}$	0.01	6.8	36	2.97	1.0	1.73
$Mg_{1.98}Li_{0.02}Si_{0.4}Sn_{0.6}$	0.02	8.4	36	3.04	1.4	1.78
$Mg_2Li_{0.03}Si_{0.4}Sn_{0.6}$	0.03	9.0	28	3.05	1.5	1.79
$Mg_{1.99}Li_{0.04}Si_{0.4}Sn_{0.6}$	0.04	9.0	31	3.01	1.4	1.78
$Mg_{1.94}Li_{0.06}Si_{0.4}Sn_{0.6}$	0.06	9.3	26	3.01	1.3	1.76

The room temperature Hall data shows an increase in charge carrier concentration with increasing Li content x both for the $Mg_2Ge_{0.4}Sn_{0.6}$ and $Mg_2Si_{0.4}Sn_{0.6}$ samples for small x and saturation for $x \geq$ 0.03. The Hall mobility μ_H decreases with increasing x.

Exemplary data from powder XRD is presented in Figure 1. The main peaks correspond to the cubic anti-fluorite structure of Mg_2Si, Mg_2Ge, and Mg_2Sn. The lattice parameter is $a = 6.611$ Å ± 0.002 Å for all $Mg_2Ge_{0.4}Sn_{0.6}$ samples. Most of the spectra also exhibit small peaks that can be identified as elemental Sn. If the Li is not incorporated completely into the lattice but can be found *e.g.,* at the grain boundaries or if some Mg is lost during synthesis the matrix material will be Mg deficient. This can be compensated by segregation of Sn, leading to the observed secondary phase peaks in the XRD data. As Mg_2Sn is less stable than Mg_2Si or Mg_2Ge [42, 43] it is plausible that elemental Sn segregates rather than Si or Ge. The results for the $Mg_2Si_{0.4}Sn_{0.6}$ samples are comparable. The theoretical density can be estimated from the refined lattice parameter and all samples listed in Table I have a relative density > 97%, with most samples > 98%.
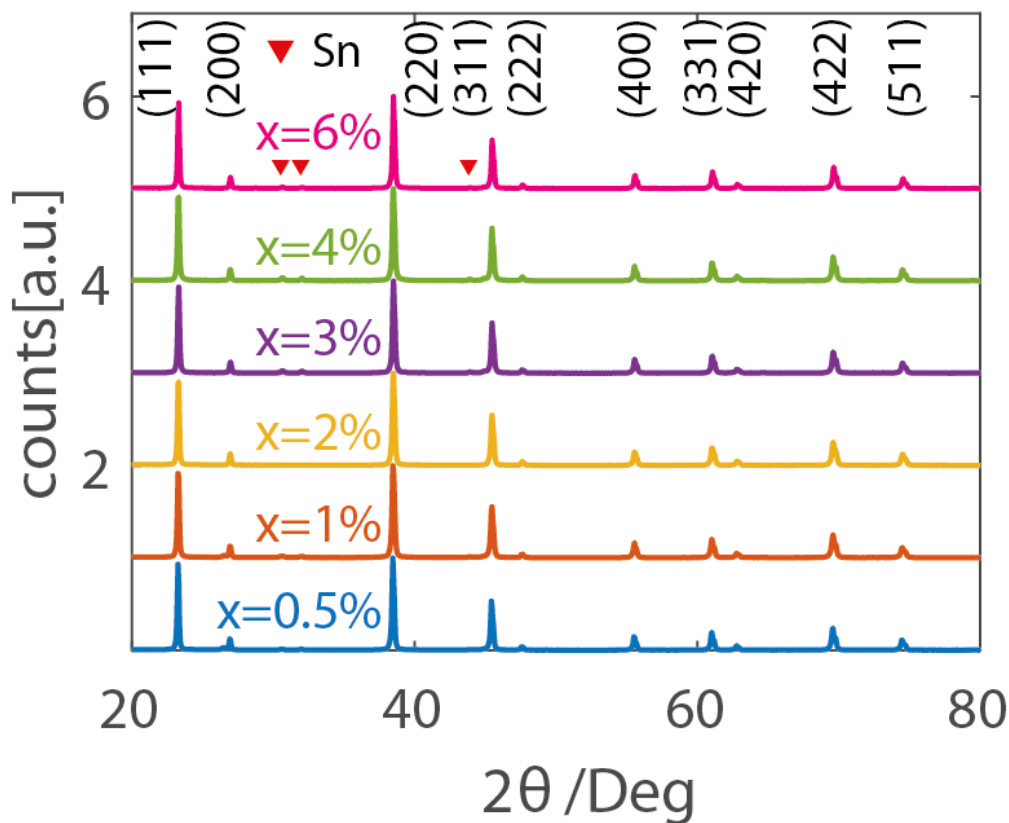

Figure 1: XRD of the $Mg_{2-x}Li_xGe_{0.4}Sn_{0.6}$ samples listed in Table I.

An SEM picture of the sample with $x = 0.03$ is shown in Figure 2. Besides the main phase in gray some bright and black spots are visible. The latter ones correspond to the little porosity of the material while the bright spots are possibly due to remains from the polishing process or due to Sn precipitates as also identified in the powder X-ray diffraction data.
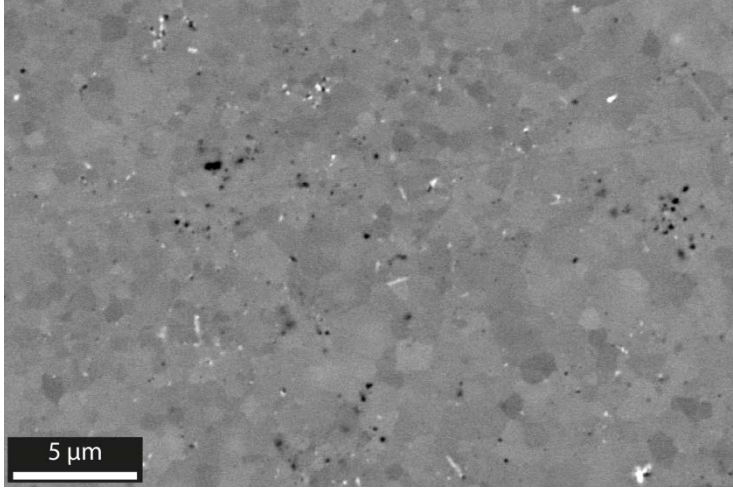
Figure 2: SEM image of sample with composition Mg$_{1.97}$Li$_{0.03}$Ge$_{0.4}$Sn$_{0.6}$ using an angle resolved backscattered electron detector.

The grains in the material show a size distribution in the 0.1 μm − 1 μm range, with the crystallites possibly being substantially smaller [36, 44]. Pointwise EDX shows a small variation in the material composition Mg$_A$Ge$_B$Sn$_C$ (Li has not been detected), with $1.985 < A < 1.996$, $0.358 < B < 0.391$, and $0.613 < C < 0.657$. The brighter grains are slightly Sn rich compared to the darker ones. This co-existence of neighboring phases with similar but distinct compositions has been observed previously for Mg$_2$Si based solid solutions [45]. However, the differences are very small so that the material will be treated as single phase material for the electronic transport discussion. We also attempted elemental analysis of the bright spots. These show a slight Mg deficiency and some Sn enrichment but the exact composition cannot be resolved due to the limited spatial resolution of the EDX. It is plausible, though, that these spots contain some elemental Sn that has also been identified in the XRD.

The thermoelectric transport data for the Mg$_{2-x}$Li$_x$Ge$_{0.4}$Sn$_{0.6}$ samples is presented in Figure 3. For better visibility error bars are shown for one sample only but are (relatively) the same for all samples. ZT was calculated from the polynomial fits of S, σ, κ that are shown as solid lines. The lattice thermal conductivity κ_{lat} (plus the bipolar contribution) is calculated from $\kappa_{\text{lat}} + \kappa_{\text{bi}} = \kappa - \kappa_{\text{e}} = \kappa - L\sigma T$, where κ_{e} is the electronic contribution to the thermal conductivity and L the Lorenz number that was calculated in the framework of a single parabolic band model, see discussion section.
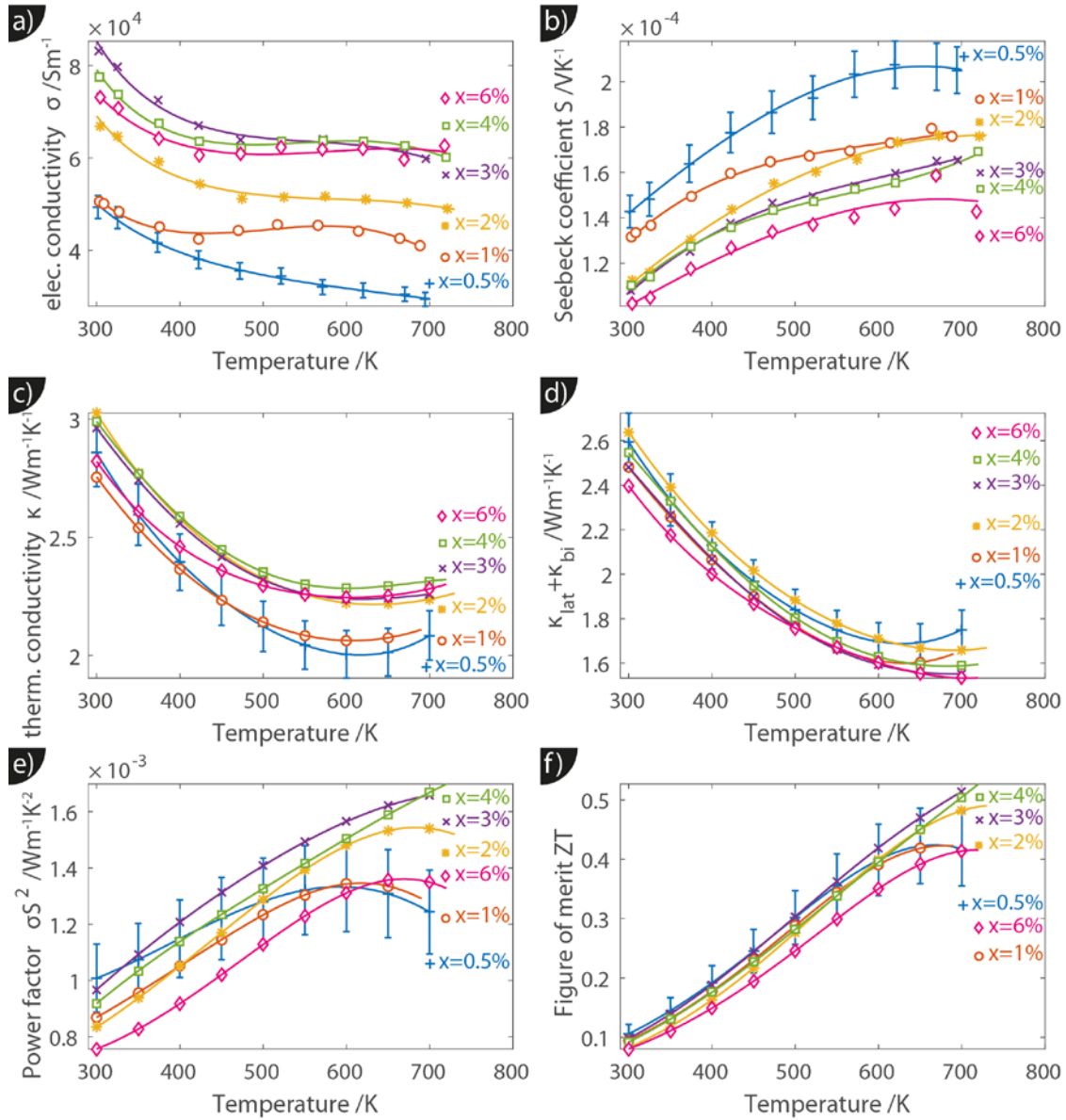
Figure 3: Thermoelectric properties of $Mg_{2-x}Li_xGe_{0.4}Sn_{0.6}$. The transport follows roughly that of a degenerate semiconductor and the effect of increasing charge carrier concentration with increasing Li content x is clearly visible. At high temperatures the bipolar contribution becomes significant, especially for the low Li concentrations.

The electrical conductivity decreases with increasing temperature for low T, while at high temperatures a plateau is observed for some samples, especially those with high Li content. The Seebeck coefficient is positive for all samples, indicating p-type conduction. The magnitude increases linearly with temperature for low temperatures, but the slope decreases with increasing T showing a clear maximum for the lowest doped sample. With increasing x, σ increases while S decrease, however for $x \geq 0.03$ the differences between the samples become small. Overall, the trends are as expected for a degenerate semiconductor, with some deviations in the temperature dependence of some of the samples. The thermal conductivity decreases with increasing temperature for all samples and shows a minimum at ≈ 600 K due to the onset of the bipolar contribution. The result for $\kappa_{lat} + \kappa_{bi}$ shows the onset of the bipolar more pronounced for the low doped samples as is expected. It can also be seen that the higher doped samples show a somewhat lower $\kappa_{lat} + \kappa_{bi}$, however, the effect is small. The highest power factors are obtained for $x = 0.03, 0.04$ and are

$\sigma S^2 \approx 1.7 \times 10^{-3}$ Wm^{-1}K^{-2} at 700 K. ZT increases with T for all samples and exceeds 0.5 for the best samples.

The thermoelectric properties of the samples containing Si instead of Ge are shown in Figure 4.
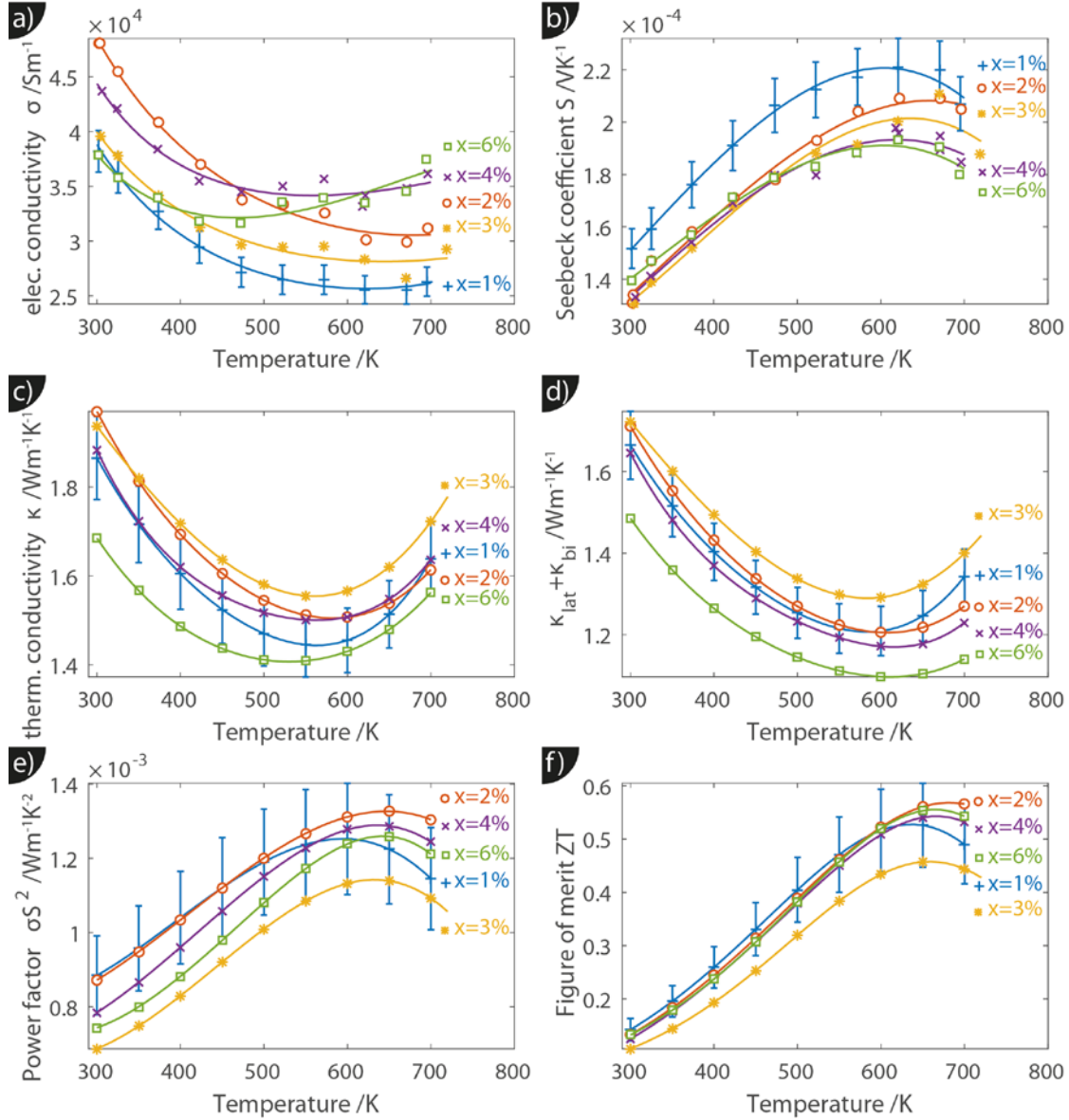

Figure 4: Thermoelectric properties of Mg$_2$Si$_{0.4}$Sn$_{0.6}$ with Li-doping. The overall trends are similar to that of the Mg$_2$Ge$_{0.4}$Sn$_{0.6}$ samples, however with lower carrier concentrations.

The overall trends are similar to the Ge-containing samples with lower σ and larger S due to lower carrier concentrations. Again, for $x \geq 0.03$ the properties of all samples are relatively similar due to similar carrier concentrations and dopant saturation. As for the Ge containing samples a small decrease of the lattice thermal conductivity is observed with increasing x. ZT exceeds 0.55 at 670 K for the best samples. In contrast to the Ge-containing samples, the maximum figure of merit is below 700 K for all samples.

4. Discussion

The Mg$_2$Ge$_{0.4}$Sn$_{0.6}$ and Mg$_2$Si$_{0.4}$Sn$_{0.6}$ samples of this study have been prepared employing the same synthesis route and compaction parameters. It is thus possible to give some indication on the effect of Sn substitution by Si/Ge on the thermoelectric properties. From Table I it can be observed that for low Li content the carrier concentrations are similar, however, they "saturate" at different values for high nominal Li contents with the Ge containing samples showing higher charge carrier concentration values. The thermoelectric properties between the two sample classes differ as they are controlled by n to a large degree but it can be seen that the (Hall) mobility μ_H is lower (at comparable n) for the Si-containing samples. This leads to lower power factors making the Si containing samples less attractive where power output in addition to efficiency is also application concern. It can also be seen that the Si-containing samples have a lower (lattice) thermal conductivity. Both effects are well known for the n-type material and are due to the higher mass contrast and atomic radius difference between Si and Sn than Ge and Sn [38, 39].

A direct comparison of the thermoelectric properties is given in Figure 5, where $\sigma S^2, \kappa_{lat} + \kappa_{bi}, ZT$ and $(ZT)_{eng}$ are given for the sample with the best thermoelectric properties ($x = 0.03$ and $x = 0.02$ for the Mg$_2$Ge$_{0.4}$Sn$_{0.6}$ and Mg$_2$Si$_{0.4}$Sn$_{0.6}$ samples, respectively). The engineering figure of

merit is given by $(ZT)_{eng} = \dfrac{\left(\int_{T_c}^{T_h} S(T)dT\right)^2}{\int_{T_c}^{T_h} \rho(T)dT * \int_{T_c}^{T_h} \kappa(T)dT}\Delta T$, with $\rho = \sigma^{-1}$, T_c the cold side temperature and

T_h the hot side temperature and $\Delta T = T_h - T_c$. While ZT evaluates the thermoelectric properties of a material at a certain temperature, $(ZT)_{eng}$ is an integral quantitiy that is closely related to a potential device efficiency [46] . It also allows for a better comparison between different materials where the temperature dependence of ZT will be different, possibly leading to wrong conclusions about material quality.
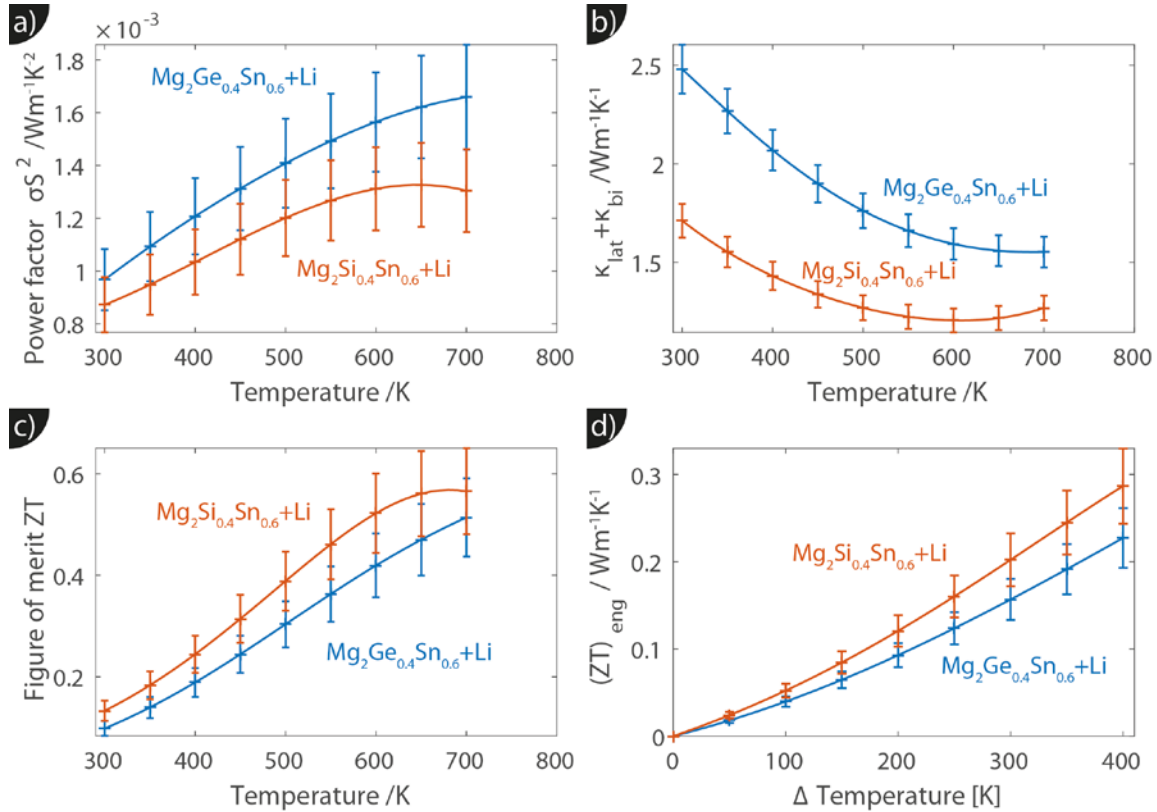
Due to the trade-off between κ_{lat} and power factor the thermoelectric figure of merit of the best Mg$_2$Ge$_{0.4}$Sn$_{0.6}$ and Mg$_2$Si$_{0.4}$Sn$_{0.6}$ sample is comparable, with the Si sample being somewhat better over the whole temperature range, which also leads to a slightly better $(ZT)_{\text{eng}}$. Furthermore, for the Si containing sample (with lower n_{H}) the detrimental influence of the bipolar effect is clearly visible leaving room for some improvement provided that the carrier concentration can be increased further. A comparison with literature data reveals that the Mg$_2$Ge$_{0.4}$Sn$_{0.6}$ samples have the highest power factor reported for p-type Mg$_2$(Si,Ge,Sn) with a maximum of 1.7×10^{-3} Wm^{-1}K^{-2} at 700 K while the best reported Mg$_2$(Si,Sn) samples have only 1.4×10^{-3} Wm^{-1}K^{-2} [35-37]. The thermoelectric figure of merit for the Mg$_2$Si$_{0.4}$Sn$_{0.6}$ samples is comparable to the previous reports with similar compositions [35-37, 42], with the optimum carrier concentration comparable to that in [37], but significantly lower than the values reported in [35, 36, 42]. Carrier mobility and lattice thermal conductivity are roughly comparable but show some variations between the different reports. This is not unexpected as both quantities are not only influenced by intrinsic material properties but also by material synthesis technique and compaction, which are different for the different reports. Some insight on fundamental material parameters can be gained by analyzing the data in the frame work of a single parabolic band model [47]. This was found to be well suitable for the n-type material [8, 48] and often assumed to be valid for the p-type material [42, 49]. However, there is some debate whether this is applicable or two or more bands should be taken into account [35, 50]. We will thus employ it but discuss exceptions from the expected behavior. The relevant equations are

$$S = -\frac{k}{e}\left(\frac{2F_1(\eta)}{F_0(\eta)} - \eta\right),$$

$$n = 4\pi\left(\frac{2m^* k_B T}{h^2}\right)^{3/2} F_{1/2}(\eta), \tag{1}$$

$$L = \frac{k^2}{e^2}\frac{3F_0 F_2 - 4F_1^2}{F_0^2}$$

Here e is the elementary charge, k_B Boltzmann's constant, F_i the Fermi integral of order i, and the reduced chemical potential η is given by $\eta = \frac{E_F}{k_B T}$. The measured Hall carrier density n_{H} is linked to the true carrier density by $n_{\text{H}} = n/r_{\text{H}}$ with the Hall scattering factor given by $r_{\text{H}} = \frac{1.5 F_{0.5} F_{-0.5}}{2F_0^2}$. The density of states (DOS) effective mass is denoted as m^*. The Lorenz number L is used to calculate the lattice thermal conductivity $\kappa_{\text{lat}} + \kappa_{\text{bi}} = \kappa - \kappa_{\text{e}} = \kappa - L\sigma T$. For the calculations we have assumed a scattering parameter of $\lambda = -0.5$, corresponding to carrier scattering by acoustic phonons being dominant, an assumption that is considered to be well fulfilled for the material at temperatures above 300 K [8, 13, 48, 51].

The density of states (DOS) effective mass m^* can be extracted from the measured Seebeck coefficient and the carrier concentration. The Seebeck versus carrier concentration (Pisarenko plot) at room temperature is shown in Figure 6. The results are given for the Mg$_2$Ge$_{0.4}$Sn$_{0.6}$ and

Mg$_2$Si$_{0.4}$Sn$_{0.6}$ samples discussed in this study, samples with compositions close to Mg$_2$Ge$_{0.25}$Sn$_{0.75}$ that were prepared using the same synthesis and compaction parameters [52], and literature results for Mg$_2$Si$_{0.4}$Sn$_{0.6}$ and Mg$_2$Si$_{0.3}$Sn$_{0.7}$ using Li as dopant [35-37].
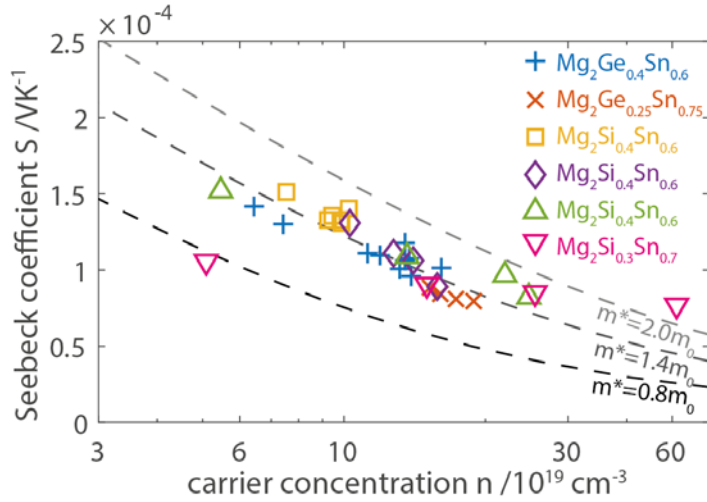
Figure 6: Pisarenko plot for samples with a composition close to Mg$_2$X$_y$Sn$_{1-y}$ (X=Si, Ge; 0.25<y<0.4) from the authors and literature reports (diamond [37], upwards triangle [36], downward triangle [35]). The dashed lines correspond to the theoretical prediction within the SPB model for fixed values of m^*. Most of the data groups around $m^* = 1.4\ m_0$.

The Mg$_2$Ge$_{0.4}$Sn$_{0.6}$ samples of the authors have an (sample average) effective mass of $m^* \approx 1.3\ m_0$ and show a good correspondence to the theoretical prediction within the SPB model. For the Mg$_2$Si$_{0.4}$Sn$_{0.6}$ samples the average value is $m^* \approx 1.5\ m_0$, indicating that replacing Si by Ge does not affect the band structure dramatically. This is due to the similarity of the crystal potentials for Si and Ge and is supported by density functional (DFT) calculations [53, 54]. Nevertheless, the higher m^* of the Mg$_2$Si$_{0.4}$Sn$_{0.6}$ samples can partially explain the observed lower mobility as $\mu \propto (m^*)^{-2.5}$ for acoustic phonon scattering [55]. Comparing Mg$_2$Ge$_{0.4}$Sn$_{0.6}$ samples with Mg$_2$Ge$_{0.25}$Sn$_{0.75}$ samples it can further be deduced that increasing the Sn content from 0.6 to 0.75 has no significant effect on the band structure, either. It can be seen that the overall fit of the experimental data to the SPB prediction with m^* is quite good even for some literature date, especially for $n \leq 10^{20}$ cm^{-3}. The data from Zhang *et al*. for Mg$_2$Si$_{0.3}$Sn$_{0.7}$ presents an exception. They observe a significantly lower effective mass for low carrier concentrations which increases dramatically for large n and have interpreted this as a proof for a non-degeneracy of the two highest valence bands and thus a varying contribution of the bands depending on carrier concentration. However, the vast majority of the data is consistent with the SPB model at least for $n < 2 \times 10^{20}$ cm^{-3}. This is specific for Li as it has been shown that for Ga-doped p-type samples a non-constant effective mass can be observed for all relevant carrier concentrations [35, 49, 56]. Comparison with literature data for Li doped samples also shows that the mobility depends strongly on the synthesis technique (at comparable carrier concentration and composition) and that the optimum carrier concentration varies significantly between the different reports. This indicates that the SPB model is not sufficient to properly predict all the thermoelectric properties of the material and further research is required.

One of the reasons why p-type Mg$_2$(Si,Ge,Sn) has remained poor previously is that for most dopants the experimentally observed hole concentration is way below the expected value. Zhang *et al*. show

that Li is much more efficient than e.g., Ga, Ag, Na ,and K [35], however it has also been noted previously that the hole concentration is also below the expected value if each Li provides one hole [35, 37]. We have therefore summarized the carrier concentration data versus nominal Li content in Figure 7. The theoretical expectation was calculated for a lattice constant of $a = 6.6 \times 10^{-10}$ m and under the assumption that each Li atom replaces one Mg atom and provides one free hole. We have used the nominal Li content as it has been shown that the difference between nominal and actual Li content is not very large [35, 37]. This is due to the high solubility of Li in $Mg_2(Si,Ge,Sn)$ [35, 57].
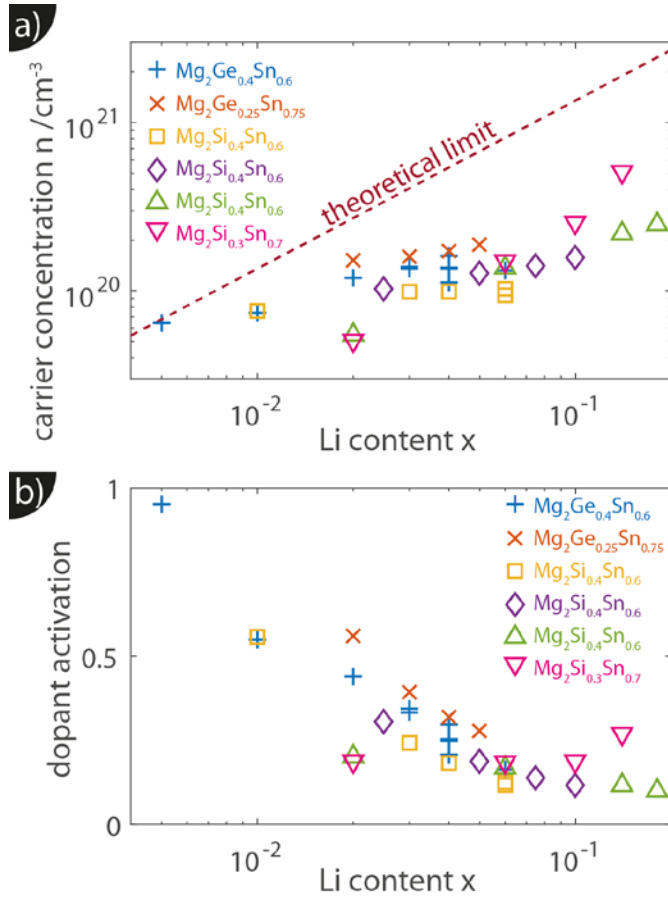

Figure 7: a) Li content x vs. experimentally determined carrier concentration for the same samples as discussed in Figure 6. The dashed line is obtained under the assumption that each Li atom provides one free hole. Although Li doping allows for high carrier concentrations, the experimentally observed values remain far below the limiting value, especially for higher x values. b) The ratio of experimental and limiting value indicates that the dopant activation increases with increasing Sn content of the samples and that replacing Si by Ge leads to a higher dopant activation.

Overall it can be seen that the dopant activation (ratio of experimental and theoretical carrier concentration) can be close to unity for low Li content but decreases approximately monotonously down to 0.1 with increasing Li content. Comparison of the samples by the authors (same synthesis technique) shows that replacing Si by Ge leads to a higher dopant activation as does increasing the Sn content in the samples. This confirms earlier reports in the literature [49] and is in line with experimental data e.g., from Ihou-Mouko et al. who showed an increase in carrier concentration going from Mg_2Si to $Mg_2Si_{0.6}Ge_{0.4}$ at the same Ga content [54]. Comparison with literature reveals that the dopant activation depends on synthesis technique and parameters, an effect directly observed e.g., by Isachenko et al., who compared polycrystalline with nanocrystaline samples [42]. Gao et al. suggested that some Li might go into interstitial position (and thus does not provide holes

as effectively as expected), but has not been confirmed experimentally [57]. The question why the dopant activation is way below unity for high Li content remains to be addressed in the future.

5. Conclusion

We have synthesized p-type $Mg_2Ge_{0.4}Sn_{0.6}$ and $Mg_2Si_{0.4}Sn_{0.6}$ samples using Li as dopant. No previous reports for Li doped $Mg_2Ge_{0.4}Sn_{0.6}$ can be found in the literature and we could obtain a peak power factor of 1.7×10^{-3} $Wm^{-1}K^{-2}$, the best value for p-type $Mg_2(Si,Ge,Sn)$. Systematic comparison between Ge and Si containing samples show that the Si containing samples have a lower power factor but also a lower lattice thermal conductivity, resulting in a slightly better thermoelectric figure of merit. Analysis of our experimental data and literature results reveals that carrier effective mass can be described within the framework of a parabolic band model and that the difference between Si and Ge containing samples is small. We could also show that the dopant activation for Li decreases monotonously with increasing Li content and moreover that replacing Si by Ge and increasing of Sn:(Si,Ge) ratio enhances the dopant activation. This indicates that material optimization for p-type $Mg_2(Si,Ge,Sn)$ is more complex than for the n-type material as the optimization of carrier concentration is not only controlled by dopant concentration but also the Si:Ge:Sn ratio in the material. This might allow for further p-type material improvement in the future.

Acknowledgements

References

[1]   GS Snyder, ES Toberer, Complex thermoelectric materials, Nat. Mater. 7 (2008) 105.
[2]   K Biswas, JQ He, ID Blum, CI Wu, TP Hogan, DN Seidman, VP Dravid, MG Kanatzidis, High-performance bulk thermoelectrics with all-scale hierarchical architectures, Nature 489 (2012) 414.
[3]   G Rogl, A Grytsiv, P Rogl, N Peranio, E Bauer, M Zehetbauer, O Eibl, n-Type skutterudites (R,Ba,Yb)(y)Co4Sb12 (R = Sr, La, Mm, DD, SrMm, SrDD) approaching ZT approximate to 2.0, Acta Mater. 63 (2014) 30.
[4]   S Sakurada, N Shutoh, Effect of Ti substitution on the thermoelectric properties of (Zr,Hf)NiSn half-Heusler compounds, Appl. Phys. Lett. 86 (2005).
[5]   LD Zhao, SH Lo, YS Zhang, H Sun, GJ Tan, C Uher, C Wolverton, VP Dravid, MG Kanatzidis, Ultralow thermal conductivity and high thermoelectric figure of merit in SnSe crystals, Nature 508 (2014) 373.
[6]   DR Brown, T Day, T Caillat, GJ Snyder, Chemical Stability of (Ag,Cu)(2)Se: a Historical Overview, J. Electron. Mater. 42 (2013) 2014.
[7]   VK Zaitsev, MI Fedorov, EA Gurieva, IS Eremin, PP Konstantinov, AY Samunin, MV Vedernikov, Highly effective Mg2Si1-xSnx thermoelectrics, Phys. Rev. B 74 (2006) 045207.
[8]   W Liu, XJ Tan, K Yin, HJ Liu, XF Tang, J Shi, QJ Zhang, C Uher, Convergence of Conduction Bands as a Means of Enhancing Thermoelectric Performance of n-Type Mg2Si1-xSnx Solid Solutions, Phys. Rev. Lett. 108 (2012) 166601.

[9]   XH Liu, TJ Zhu, H Wang, LP Hu, HH Xie, GY Jiang, GJ Snyder, XB Zhao, Low Electron Scattering Potentials in High Performance Mg2Si0.45Sn0.55 Based Thermoelectric Solid Solutions with Band Convergence, Adv. Energy Mater. 3 (2013) 1238.

[10]   W Liu, X Tang, J Sharp, Low-temperature solid state reaction synthesis and thermoelectric properties of high-performance and low-cost Sb-doped Mg2Si0.6Sn0.4, J. Phys. D: Appl. Phys. 43 (2010) 085406.

[11]   AU Khan, NV Vlachos, E Hatzikraniotis, GS Polymeris, CB Lioutas, EC Stefanaki, KM Paraskevopoulos, I Giapintzakis, T Kyratsi, Thermoelectric properties of highly efficient Bi-doped Mg2Si1-x-ySnxGey materials, Acta Mater. 77 (2014) 43.

[12]   P Gao, I Berkun, R Schmidt, M Luzenski, X Lu, P Bordon Sarac, E Case, T Hogan, Transport and Mechanical Properties of High-ZT Mg2.08Si0.4–x Sn0.6Sb x Thermoelectric Materials, J. Electron. Mater. 43 (2013) 1790.

[13]   T Dasgupta, C Stiewe, J de Boor, E Müller, Influence of power factor enhancement on the thermoelectric figure of merit in Mg2Si0.4Sn0.6 based materials, physica status solidi (a) (2014) 1250.

[14]   S LeBlanc, SK Yee, ML Scullin, C Dames, KE Goodson, Material and manufacturing cost considerations for thermoelectrics, Renew. Sust. Energ. Rev. 32 (2014) 313.

[15]   SK Bux, MT Yeung, ES Toberer, GJ Snyder, RB Kaner, JP Fleurial, Mechanochemical synthesis and thermoelectric properties of high quality magnesium silicide, J. Mater. Chem. 21 (2011) 12259.

[16]   JB Zhao, ZX Liu, J Reid, K Takarabe, T Iida, BS Wang, U Yoshiya, JS Tse, Thermoelectric and electrical transport properties of Mg2Si multi-doped with Sb, Al and Zn, Journal of Materials Chemistry A 3 (2015) 19774.

[17]   J de Boor, S Gupta, H Kolb, t Dasgupta, E Mueller, Thermoelectric transport and microstructure of optimized Mg2Si0.8Sn0.2, J. Mater. Chem. C 3 (2015) 10467.

[18]   J de Boor, C Gloanec, H Kolb, R Sottong, P Ziolkowski, E Müller, Fabrication and characterization of nickel contacts for magnesium silicide based thermoelectric generators, J. Alloys Compd. 632 (2015) 348.

[19]   A Ferrario, S Battiston, S Boldrini, T Sakamoto, E Miorin, A Famengo, A Miozzo, S Fiameni, T Iida, M Fabrizio, Mechanical and electrical characterization of low-resistivity contact materials for Mg2Si, Mater. Today-Proc. 2 (2015) 573.

[20]   T Sakamoto, Y Taguchi, T Kutsuwa, K Ichimi, S Kasatani, M Inada, Investigation of Barrier-Layer Materials for Mg2Si/Ni Interfaces, J. Electron. Mater. 45 (2015) 1321.

[21]   T Sakamoto, T Iida, Y Honda, M Tada, T Sekiguchi, K Nishio, Y Kogo, Y Takanashi, The Use of Transition-Metal Silicides to Reduce the Contact Resistance Between the Electrode and Sintered - Type Mg2Si, J. Electron. Mater. 41 (2012) 1805.

[22]   J de Boor, D Droste, C Schneider, J Janek, E Mueller, Thermal Stability of Magnesium Silicide/Nickel Contacts, J. Electron. Mater. (2016) 1.

[23]   HS Kim, K Kikuchi, T Itoh, T Iida, M Taya, Design of segmented thermoelectric generator based on cost-effective and light-weight thermoelectric alloys, Mater. Sci. Eng. B-Adv. Funct. Solid-State Mater. 185 (2014) 45.

[24]   T Nakamura, K Hatakeyama, M Minowa, Y Mito, K Arai, T Iida, K Nishio, Power-Generation Performance of a pi-Structured Thermoelectric Module Containing Mg2Si and MnSi1.73, J. Electron. Mater. 44 (2015) 3592.

[25]   T Nemoto, T Iida, J Sato, H Suda, Y Takanashi, Improvement in the Durability and Heat Conduction of uni-leg Thermoelectric Modules Using n-type Mg2Si Legs, J. Electron. Mater. 43 (2014) 1890.

[26]   T Sakamoto, T Iida, Y Ohno, M Ishikawa, Y Kogo, N Hirayama, K Arai, T Nakamura, K Nishio, Y Takanashi, Stress Analysis and Output Power Measurement of an n-Mg2Si Thermoelectric Power Generator with an Unconventional Structure, J. Electron. Mater. 43 (2014) 1620.

[27]   G Skomedal, L Holmgren, H Middleton, IS Eremin, GN Isachenko, M Jaegle, K Tarantik, N Vlachos, M Manoli, T Kyratsi, D Berthebaud, NY Dao Truong, F Gascoin, Design, assembly and characterization of silicide-based thermoelectric modules, Energy Convers. Manage. 110 (2016) 13.

[28]   KR Tarantik, JD König, M Jägle, J Heuer, J Horzella, A Mahlke, M Vergez, K Bartholomé, Thermoelectric Modules Based on Silicides – Development and Characterization, Materials Today: Proceedings 2 (2015) 588.

[29]   VK Zaitsev, MI Federov, IS Eremin, EA Gurieva. Thermoelectrics on the Base of Solid Solutions of Mg2B IVCompounds. In: Rowe DM, editor. Thermoelectrics Handbook: Macro to Nano. Boca Raton, USA: CRC, 2005.

[30]   MI Fedorov, VK Zaitsev. Silicide Thermoelectrics: State of the Art and Prospects. In: Rowe DM, editor. Thermoelectrics and its Energy Harvesting: Modules, Systems, and Applications in Thermoelectrics. Boca Raton, FL: CRC Press,Taylor & Francis Group, 2012.

[31]   J-i Tani, H Kido, Fabrication and thermoelectric properties of Mg2Si-based composites using reduction reaction with additives, Intermetallics 32 (2013) 72.

[32]   T Sakamoto, T Iida, A Matsumoto, Y Honda, T Nemoto, J Sato, T Nakajima, H Taguchi, Y Takanashi, Thermoelectric Characteristics of a Commercialized Mg2Si Source Doped with Al, Bi, Ag, and Cu, J. Electron. Mater. 39 (2010) 1708.

[33]   A Prytuliak, E Godlewska, K Mars, D Berthebaud, Synchrotron Study of Ag-Doped Mg2Si: Correlation Between Properties and Structure, J. Electron. Mater. 43 (2014) 3746.

[34]   Y Isoda, S Tada, T Nagai, H Fujiu, Y Shinohara, Thermoelectric Properties of p-Type Mg2.00Si0.25Sn0.75 with Li and Ag Double Doping, J. Electron. Mater. 39 (2010) 1531.

[35]   Q Zhang, L Cheng, W Liu, Y Zheng, X Su, H Chi, H Liu, Y Yan, X Tang, C Uher, Low effective mass and carrier concentration optimization for high performance p-type Mg2(1-x)Li2xSi0.3Sn0.7 solid solutions, PCCP 16 (2014) 23576.

[36]   X Tang, G Wang, Y Zheng, Y Zhang, K Peng, L Guo, S Wang, M Zeng, J Dai, G Wang, X Zhou, Ultra rapid fabrication of p-type Li-doped Mg2Si0.4Sn0.6 synthesized by unique melt spinning method, Scripta Mater. 115 (2016) 52.

[37]   P Gao, JD Davis, VV Poltavets, TP Hogan, The p-type Mg2LixSi0.4Sn0.6 thermoelectric materials synthesized by a B2O3 encapsulation method using Li2CO3 as the doping agent, J. Mater. Chem. C 4 (2016) 929.

[38]   W Liu, HS Kim, S Chen, Q Jie, B Lv, M Yao, Z Ren, CP Opeil, S Wilson, C-W Chu, Z Ren, n-type thermoelectric material Mg2Sn0.75Ge0.25 for high power generation, PNAS 112 (2015) 3269.

[39]   J Mao, HS Kim, J Shuai, Z Liu, R He, U Saparamadu, F Tian, W Liu, Z Ren, Thermoelectric properties of materials near the band crossing line in Mg2Sn–Mg2Ge–Mg2Si system, Acta Mater. 103 (2016) 633.

[40]   T Dasgupta, C Stiewe, R Hassdorf, AJ Zhou, L Boettcher, E Mueller, Effect of vacancies on the thermoelectric properties of Mg2Si1-xSbx (0 <= x <= 0.1), Phys. Rev. B 83 (2011) 235207.

[41]   HS Wang, SQ Bai, LD Chen, A Cuenat, G Joshi, H Kleinke, J Konig, HW Lee, J Martin, MW Oh, WD Porter, ZF Ren, J Salvador, J Sharp, P Taylor, AJ Thompson, YC Tseng, International Round-Robin Study of the Thermoelectric Transport Properties of an n-Type Half-Heusler Compound from 300 K to 773 K, J. Electron. Mater. 44 (2015) 4482.

[42]   GN Isachenko, AY Samunin, EA Gurieva, MI Fedorov, DA Pshenay-Severin, PP Konstantinov, MD Kamolova, Thermoelectric Properties of Nanostructured p-Mg2SixSn1-x (x=0.2 to 0.4) Solid Solutions, J. Electron. Mater. 45 (2016) 1982.

[43]   DW Zhou, JS Liu, SH Xu, P Peng, Thermal stability and elastic properties of Mg2X (X = Si, Ge, Sn, Pb) phases from first-principle calculations, Computational Materials Science 51 (2012) 409.

[44]   Z Liu, J Shuai, J Mao, Y Wang, Z Wang, W Cai, J Sui, Z Ren, Effects of antimony content in MgAg0.97Sbx on output power and energy conversion efficiency, Acta Mater. 102 (2016) 17.

[45]   G Bernard-Granger, C Navone, J Leforestier, M Boidot, K Romanjek, J Carrete, J Simon, Microstructure investigations and thermoelectrical properties of an N-type magnesium-silicon-tin alloy sintered from a gas-phase atomized powder, Acta Mater. 96 (2015) 437.

[46]   HS Kim, W Liu, G Chen, C-W Chu, Z Ren, Relationship between thermoelectric figure of merit and energy conversion efficiency, PNAS 112 (2015) 8205.

[47]   AF May, GJ Snyder. Introduction to Modeling Thermoelectric Transport at High Temperatures. In: Rowe DM, editor. Thermoelectrics and its Energy Harvesting: Materials, Preparation, and Characterization in Thermoelectrics. CRC Press, 2012.

[48]   W Liu, H Chi, H Sun, Q Zhang, K Yin, X Tang, Q Zhang, C Uher, Advanced thermoelectrics governed by a single parabolic band: Mg2Si0.3Sn0.7, a canonical example, PCCP 16 (2014) 6893.

[49]   W Liu, K Yin, X Su, H Li, Y Yan, X Tang, C Uher, Enhanced hole concentration through Ga doping and excess of Mg and thermoelectric properties of p-type Mg2(1+z)(Si0.3Sn0.7)(1-y)Ga-y, INTERMETALLICS 32 (2013) 352.

[50]   K Kutorasinski, B Wiendlocha, J Tobola, S Kaprzyk, Importance of relativistic effects in electronic structure and thermopower calculations for Mg2Si, Mg2Ge, and Mg2Sn, Phys. Rev. B 89 (2014) 115205.

[51]   J Mao, Y Wang, B Ge, Q Jie, Z Liu, U Saparamadu, W Liu, Z Ren, Thermoelectric performance enhancement of Mg2Sn based solid solutions by band convergence and phonon scattering via Pb and Si/Ge substitution for Sn, PCCP (2016).

[52]   U Saparamadu, J De Boor, J Mao, ZF Ren. manuscript in preparation. 2016.

[53]   K Mars, H Ihou-Mouko, G Pont, J Tobola, H Scherrer, Thermoelectric Properties and Electronic Structure of Bi- and Ag-Doped Mg2Si1−x Ge x Compounds, J. Electron. Mater. 38 (2009) 1360.

[54]   H Ihou-Mouko, C Mercier, J Tobola, G Pont, H Scherrer, Thermoelectric properties and electronic structure of p-type Mg2Si and Mg2Si0.6Ge0.4 compounds doped with Ga, J. Alloys Compd. 509 (2011) 6503.

[55]   C Wood, MATERIALS FOR THERMOELECTRIC ENERGY-CONVERSION, Rep. Prog. Phys. 51 (1988) 459.

[56]   GN Isachenko, VK Zaitsev, MI Fedorov, AT Burkov, EA Gurieva, PP Konstantinov, MV Vedernikov, Kinetic properties of p-Mg2Si (x) Sn1-x solid solutions for x < 0.4, Physics of the Solid State 51 (2009) 1796.

[57]   P Nieroda, A Kolezynski, M Oszajca, J Milczarek, KT Wojciechowski, Structural and Thermoelectric Properties of Polycrystalline p-Type Mg2-x Li (x) Si, J. Electron. Mater. 45 (2016) 3418.